The Cartesian Diver: A Self-Profiling Lagrangian Velocity Recorder

T. F. DUDA, C. S. COX AND T. K. DEATON

Scripps Institution of Oceanography, La Jolla, California

(Manuscript received 5 February 1987, in final form 15 June 1987)

ABSTRACT

The Cartesian diver is an autonomous velocity profiler capable of operating to 1 km depth in the ocean. It has a self-controlled buoyancy changer which is used to control the direction of profiling. The buoyancy changer has two states, full positive or full negative buoyancy. With correct ballasting the instrument has roughly equal up and down profiling speeds. A passive compressible volume appended to the pressure case is used to keep the buoyancy constant during an up or down run despite changes of density of the surrounding seawater, thus keeping the profiling speed and sampling intervals constant throughout a profile. A microcomputer system controls the buoyancy changer, data collection, and internal recording. Battery energy storage for the buoyancy changer is sufficient for 200 consecutive dives to 500 meters, thus 400 profiles. Horizontal components of velocity fluctuations with vertical wavelengths greater than 10 m are sensed using the method of geomagnetic induction. Since the instrument cannot accelerate relative to the fluid surrounding it, changes of its vertical velocity can be measured with a pressure gauge and interpreted as oceanic vertical velocity. Temperature, conductivity and microscale conductivity probes are included, in order to investigate relationships between finescale velocity structure, finescale density structure, and diffusive scale conductivity structure.

1. Introduction

Vertical profiles of oceanic horizontal velocity have been collected for over a decade. Many techniques have been used. For example, drifting, descending floats have been tracked acoustically (Spain et al., 1981; Luyten et al., 1982), velocity relative to a free-fall instrument has been measured (Evans et al., 1979), and these techniques have been combined (Hayes et al., 1984). Doppler acoustic return from natural scatterers has been recorded (Pinkel, 1980; Regier, 1982), velocity has been inferred from baroclinically induced electric fields in the ocean (Sanford et al., 1978; Sanford et al., 1982), and a current meter of variable buoyancy has been tethered to a mooring (Eriksen et al., 1982). The Cartesian-diver electromagnetic profiler extends profiling capabilities in the upper ocean by allowing economical and rapidly repeated profiling, like Doppler sonar, but with vertical wavenumber resolution to scales less than 10 m vertically. In addition, vertical velocities can be concurrently measured, and sampling intervals are variable in space and time and can be chosen to optimize the study of inertial motions, buoyancy waves, turbulence, and persistent shears. Finally, the device makes a Lagrangian measurement of the flow field because it is advected with the flow and remains in a distinct volume of fluid.

The Cartesian diver can operate in the upper 1000 meters of the ocean. It is an untethered autonomous device which alternately falls and rises freely through multiple cycles, recording data internally. The diver propels itself vertically by adjusting its volume while its mass is unchanged, thereby changing its buoyancy. The name is drawn from the toy made from an inverted bottle in which the buoyancy can be controlled by compression of an enclosed volume of gas while it is submerged in a liquid. The device was used prior to Descartes to illustrate the incompressibility of water relative to air (Magiotti, 1648), but Descartes name has since been associated with it. The oceanic Cartesian diver has been engineered primarily to record continuous profiles of horizontal velocity using a variation of the method of geomagnetic induction. This is the method used by the profilers of Sanford et al. (1978) and Sanford et al. (1982).

With diver horizontal velocity estimation, the assumption is made that the ocean electric field $\mathbf{E}_s$ measured in a stationary coordinate system does not vary with depth. Consequently the electric field measured in the reference frame of a drifter, $\mathbf{E}' = \mathbf{E}_s + \mathbf{V} \times \mathbf{B}$, yields the drifter velocity $\mathbf{V}$. Here $\mathbf{B}$ is the local magnetic induction. The diver records the horizontal components of the apparent electric field, which includes the effect of all three components of the diver's velocity. If the instrument moves horizontally at the same speed as the surrounding fluid, and if its vertical velocity is steady or known, then vertical shear of horizontal velocity is directly determined from vertical variations of the measured horizontal electric field. The proximity of the diver's horizontal velocity to that of the local

Corresponding author address: Institute of Marine Sciences, University of California, Santa Cruz, CA 95064

water appears to be sufficient, based on numerical simulations.

The vertical velocity of the water is measured by observing the vertical velocity of the instrument relative to the surface with a pressure gauge. Since the package profiles at terminal velocity, changes in its falling or rising rate can be attributed to the vertical motion of the surrounding fluid. Concurrent profiles of other parameters can be gathered by attaching additional sensors. The chosen configuration includes a metal alloy temperature sensor and a conductivity cell for density measurements, and a microscale conductivity cell designed to measure fluctuations between 5 and 320 mm wavelength. The newest instrument has all functions controlled by an onboard microcomputer system. That configuration will be described here.

The diver is a quasi-Lagrangian drifter in the horizontal, in the sense that it moves with the mean velocity of the water through which it profiles. Because it profiles through a sheared horizontal velocity field it cannot follow the water at any depth in a horizontally Lagrangian manner, even if instantaneously perfectly Lagrangian in the horizontal. The Lagrangian character distinguishes the diver from moored instruments, past which there is continual advection, and from instruments which profile from a ship moving through the water. One appropriate use for the diver is study of the evolution of properties of a water mass. Another is the determination of statistical differences between separate water masses, such as variations of the internal wavefield on either side of a front (Duda and Cox, 1987).

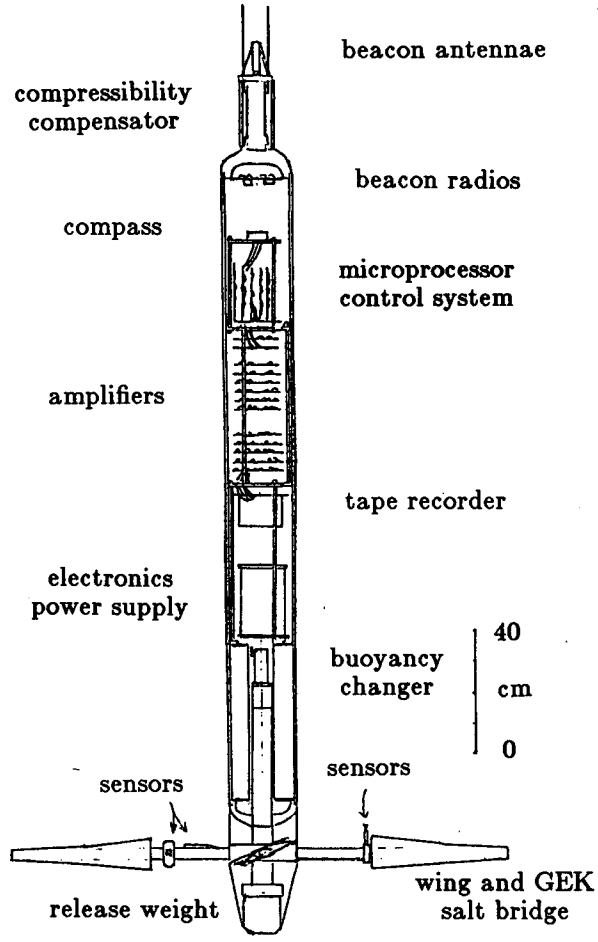

FIG. 1. Side view of the Cartesian diver profiler.

2. Instrument design

a. Overall configuration

Since the Cartesian diver must have nearly neutral buoyancy and must carry its own energy supply for vertical propulsion, it is of lightweight construction. To allow as many profiles as possible with limited energy it must have minimum vertical drag, enabling profiling with small buoyant forces. Horizontal drag must be high to allow approximately Lagrangian horizontal drifting at the chosen profiling velocities, since the local electric field is measured and the inductive horizontal velocity profiles are calculated under that assumption. In addition, section 2c, the instrument must spin as it profiles to measure successfully the local electric field (see section 2c). To satisfy these requirements the Cartesian diver is constructed from a cylindrical aluminum pressure case with an aspect ratio of length to radius of 20, with four radial wings adding horizontal drag and governing rotation (Fig. 1).

Five additional considerations contribute to the design of the diver. One is that it be easy to handle at sea. The second is that it be built of sensible and available materials. The final considerations are the speed, depth, and endurance of profiling.

The endurance of the instrument as an autonomous profiler is established by the energy supply in the form of batteries in relation to the energy required to change the volume needed to profile. The energy available to drive the buoyancy changing system can be parametrized as

$$E = lr^2\pi\rho F_e C_b F_t, \tag{1}$$

which can be rewritten

$$E = Ar^3\pi\rho F_e C_b F_t, \tag{2}$$

where $A \equiv l/r$ is the aspect ratio, l the case length, r the case radius, and ρ the density of the instrument (sea water density in this application); F_e is the fraction of instrument mass available for buoyancy changer batteries, and is determined by the pressure case material and configuration; C_b is the energy content per unit mass of the batteries at 20°C, and F_t a factor used to adjust the energy content of the batteries for a different operating temperature.

Despite the fact that the instrument has the complicated form of four radial wings about a vertical cylinder, we can approximate vertical drag with the expression for form drag

$$D = \frac{1}{2} r^2 \pi \rho U_z^2 C_D, \tag{3}$$

where U_z is the vertical velocity of the instrument, and C_D is the nondimensional drag coefficient, including the effect of the wings. Equation (3) makes sense if the wing area is proportional to the radius of the pressure case. For the latest Cartesian diver configuration, C_D has been found to be about 6.4. It is greatly influenced by the wing pitch, and is adjustable over a range of roughly 40% of its value. Work done on the water by drag forces during N profiles between the surface and H meters depth is

$$W = 2N \int_0^H D dz. \tag{4}$$

Assuming uniform drag and vertical motion, we have

$$W = 2NDH. \tag{5}$$

The buoyancy changer must perform this amount of work in order to propel the diver. The energy that must be supplied to the buoyancy changer is given by

$$E_1 = \frac{W}{q/M}, \tag{6}$$

where $q \leqslant 1$ is the efficiency of the buoyancy changer mechanism while operating under load at depth, $M \geqslant 1$ is the dive efficiency parameter, the ratio of energy used by the mechanism during a complete profiling cycle to energy used performing work at depth. M is quite variable for different buoyancy changer designs with the same efficiency at depth. For example, this parameter allows substitution of an electromechanical brake for a ratchet to lock the system, (the brake would contribute a power drain independent of the mechanical efficiency of the changer).

Setting E equal to E_1, we find the expression

$$r = \frac{NHU_z^2 C_D}{AF_e C_b F_t (q/M)}. \tag{7}$$

This is the expression relating the size, shape and design of the Cartesian diver to its profiling capabilities. Notice that r is proportional to NH, the total vertical distance covered. The distance NH is more fundamentally related to the size of the instrument than either N or H. An assumption here is that efficiency is not a function of H, which is allowable since different buoyancy changer designs can be utilized for different lower turnaround depths. Increasing A will allow faster profiling or a greater number of profiles for a specific radius, since the instrument would then carry more energy but would not encounter any more drag (in our theory, at least); U_z^2 is related to the radius in the same manner as NH. The expression also indicates that more profiling work can be accomplished with a larger instrument since forces vary with r^2 and energy content varies with r^3, assuming a constant aspect ratio.

Extruded aluminum tubing was selected for the pressure case, with internal rings preventing collapse of the out-of-round, unmachined cylinder. Hemispherical cast aluminum end caps were also chosen. This type of case typically has a mass equal to 45% of its displacement for loads up to 10 MPa, so reserving 40% of the instrument's displacement for other components gives $F_e = 0.15$. Alkaline D-cells were chosen to drive the buoyancy changer. They have $C_b = 3.3 \times 10^5$ J kg^{-1}, with a conservative estimate for F_t at 7°C of 0.5. The buoyancy changer efficiency will be assumed to be 30% for design purposes, and M will be assumed to have the conservative value of 2. The foregoing choices for the mechanical design of the Cartesian diver determine the relationship between the size and the profiling parameters. A 0.11 m radius tube allows 200 profiles to 500 meters depth at 0.12 m s^{-1} vertical velocity, for 19 days of continuous profiling. The NH value of 10^5 meters for this size instrument accurately describes the distance that can be profiled, regardless of lower turnaround depth, as long as the buoyancy changer efficiency remains at 30%.

The Cartesian diver pressure cases have been fabricated from 8 inch schedule 40 aluminum pipe. This has a radius of 0.109 m and a wall thickness of 8 mm (5/16 in.). The material is 6061-T6511 alloy, hard anodized and epoxy coated. The tubing has been machined only at O-ring sealing surfaces. The three internal stabilizing rings, made of 7075 alloy, are at 0.45 m intervals. Tubing length is 2.04 m (80 in.). The design has been tested to 14 MPa, or 2000 psi, roughly 1400 m depth. With the end assemblies in place and with an expendable ballast "drop weight" attached at the lower end the instrument has a total length of about 3 meters, and a total mass of 90 kilograms. The drop weight is released by venting a vacuum chamber which holds on the weight. The venting is performed at a prearranged time by two redundant explosive devices activated by countdown timers. At this time profiling is suspended and the instrument floats to the surface, extending two beacon radio antennae well out of the water.

Silver-silver chloride electrodes are used to sense the induced potentials. They provide a stable, low noise connection to the surrounding seawater. During velocity profiling the electric potentials to be measured are of microvolt level, while the measurement electrodes have a red noise spectrum, which can be approximated by $S_{nn} = 10^{-14}/\omega^{3/2}$ V^2 (rad s^{-1})$^{-1}$ at 0.25 rad s^{-1} (0.04 Hz) (Filloux, 1973). This noise spectrum is quite similar in shape and magnitude to the signal spectrum that would be sensed if the diver simply profiled and recorded the potentials due to its horizontal drift, without spinning. The electrodes also have a thermal coefficient of 0.4 mV °C^{-1} (Petiau and Dupis, 1980), which will create error voltages if the electrodes change temperature relative to one another or if that coefficient varies between members of an electrode pair.

To record the induced voltage signal despite the red noise and to achieve 5 meter resolution of velocity the electrodes must be physically interchanged at 0.03 Hz or faster, in as short a vertical distance as possible (at a high wavenumber). This is a modulation of the signal spectrum into the frequency (wavenumber) of rotation. Higher modulation frequency and higher modulation wavenumber each give smaller effective rms noise velocity and better resolution of the velocity. Further details of velocity resolution will be discussed in section 2c. The interchange of the electrodes is accomplished by spinning the instrument with the four previously mentioned wings, which have a span of 1.60 m. Adjustment of the wings allows profiling velocity variation over a range ±20% of the nominal velocity.

The wings are made of epoxy-fiberglass skin over polyethylene pipe. The foil sections are symmetrical, in order to have the same lift and drag characteristics for both rising and falling motion. To minimize the temperature difference voltages and to provide insulation from the changing temperature of the passing seawater, the electrodes are mounted within a 0.05 m tall, 0.11 m diameter cylindrical heat sink made of aluminum and PVC. The electrical conducting paths from the ocean to the electrodes extend through the polyethylene wing pipes, filled with agar and seawater, which serve as salt bridges, extending the effective electrode positions away from the pressure case. Effective 1.6 meter electrode separation, rather than the 0.22 meter case diameter, provides voltage gain and allows a measurement of the motionally induced voltage uninfluenced by the presence of the instrument body (Sanford et al., 1978). The resistance of each salt bridge is about 500 ohms, contributing insignificant thermal agitation noise of 3.0 nV rms in each of the two voltage channels, over the 0.25 Hz bandwidth of the instrument. The lattices of agar suppress noise by preventing water of varying conductivity from flowing into and out of the salt bridges.

Buoyancy is changed by moving a piston which seals a cylinder extending through the bottom end cap. The recovery release assembly is attached to the lower end of the cylinder. The lower end of the cylinder is open to seawater. This system is similar to that fitted to the yo-yo isotherm follower of Cairns and Williams (1976). Since the density of seawater changes rapidly through the thermocline and the instrument is virtually incompressible, a passive compensation piston at the top end of the diver is used to give the entire instrument roughly the same compressibility as seawater as both temperature and pressure vary in that region. Without the compensation the Cartesian diver would fall at an ever decreasing rate throughout its descent, and would rise at an increasing rate. The buoyancy changer and the compressibility equalizer are discussed in more detail in the next section.

The major electronic components inside the pressure case are the analog circuitry, the computer system, the tape recorder, the buoyancy changer and the battery supplies (Figs. 1 and 2). There is relatively little crowding and each of these assemblies can be upgraded or replaced without major redesign of the entire instrument. The diver is equipped with beacon radios and a programmable underwater acoustic transponder to facilitate recovery.

b. Buoyancy control

One feature of untethered profiles is that they have constant and reproducible dynamics. Since they fall and rise at a characteristic terminal velocity, the force required to propel them is equal to the drag at that velocity. Under the assumptions that the Cartesian diver has the same drag coefficient while rising as while falling and that it is ballasted to be neutrally buoyant when the buoyancy changing piston is at the midpoint of its stroke, we have the relation

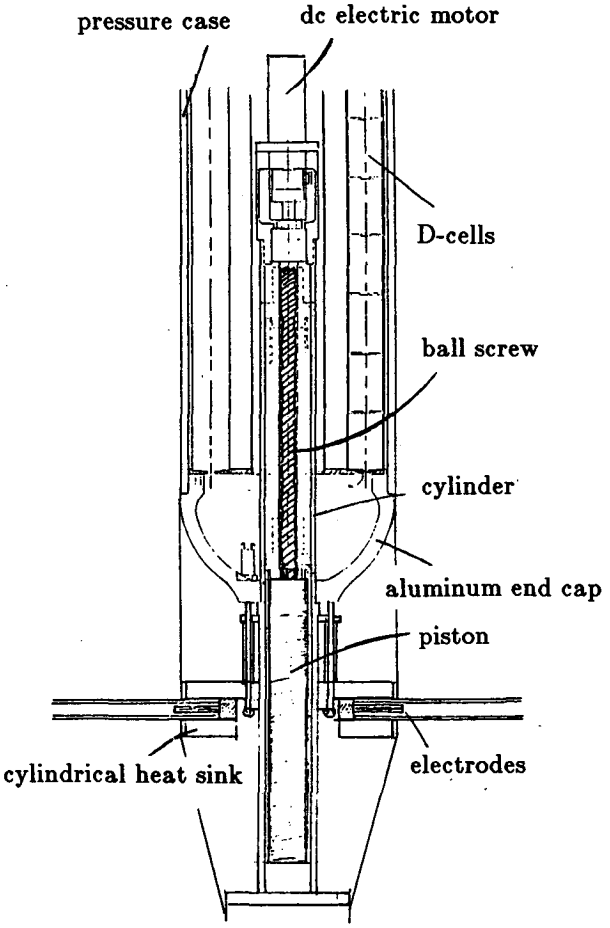

FIG. 2. Cross section of the lower end of the diver, showing the electrodes within two salt bridges within the disklike heat sink. The ball screw driven volume changer piston is shown in extended position; 12 columns of 8 D-cells each surround the buoyancy changing mechanism, supplying its energy and contributing strongly to the diver's righting moment.

$$\Delta V\rho g = \pi r^2 \rho U_z^2 C_D = 2D, \quad (8)$$

where ΔV is the displacement of the buoyancy changer. Using the previously given values of $r = 0.11$ m, $U_z = 0.12$ m s^{-1}, and $C_D = 6.4$, ΔV must be 0.00036 m^3, or 0.36 L. The instrument has been constructed with ΔV equal to 400 ml, allowing a 4 newton variation of buoyant force.

The piston is sealed with a sealing ring of the type used in hydraulic cylinders. A 25 watt, 12 000 rpm dc electric motor with a highly efficient 647:1 reduction gear drives the piston through a ball screw jack. An electromechanical brake (servo controlled) must be energized to physically release the motor for motion. This is an integral element of the most recently used motor type. Both the motor and brake voltage regulators are of the switching type in order to conserve battery energy. Overall efficiency of conversion of electrical energy to mechanical work at 3.7 MPa pressure has been measured to be 32%. The motor power regulator can control retraction of the piston at pressures up to 2 MPa. Retraction to sink at depths with great pressures is accomplished by automatically switching a resistive load across the motor. The zero efficiency piston retraction and two electromechanical brake releases per dive combine to give a dive efficiency parameter M of 2. The buoyancy changer is controlled by the computer, and the decision making can be based on any measured parameter, for example pressure, temperature, or time. The buoyancy is always changed to its maximum or minimum value, so that the instrument can only rise or fall at its maximum speed.

The bore and stroke of the volume changer are determined by the operating pressure and the characteristics of the motor and ball screw. The motor has a maximum intermittent operating torque of 0.021 N-m (2.9 oz-in.), which is transferred through the reduction gear with 81% efficiency, delivering 10.7 N-m torque to the ball screw. The ball screw has a pitch of 5 mm. The maximum allowable force is then 1.35×10^4 N. With the maximum operating depth chosen to be 1000 m, where the pressure is approximately 10^7 Pa, the correct piston radius would be 20.6 mm. The actual cylinder bore is 45.72 mm (1.800 in.), giving a piston radius of 22.9 mm. The stroke required for a 400 ml volume change is then 0.24 m.

To simplify statistical analysis of repetitive profiles, it is desirable for the Cartesian diver to move at a constant vertical velocity. The buoyant forces which propel the instrument are determined by the difference in density between the instrument and the water surrounding it. Density adjustments are made with the buoyancy changer only as the instrument changes direction, but during the course of a profile the density difference between the instrument and the seawater must remain constant. The density of seawater increases more rapidly with pressure than that of the aluminum pressure case. To compensate for this, a highly compressible volume of gas is added to the instrument to make its overall compressibility more similar to that of seawater.

The optimum compressibility equalizer for a chosen profiling depth range is determined by first selecting standard conditions near those of an intermediate profiling depth. Minimization of the rate of change of density error at this pressure and temperature yields the volume ratio $\beta = V_{g0}/V_{p0}$, the ratio of gas volume to pressure case volume under standard conditions. The density error is $\epsilon(z) = \rho_i - \rho_w$, where ρ_i is the density of the instrument $\rho_i(z) = M_i[V_p + V_g(z)]^{-1}$. Since the gas will expand above the depth of standard pressure, the expanded size of the gas volume, $V_{g\max} = \gamma V_{g0}$, will be determined by the upper depth limit of equalization, through use of Boyle and Charles' laws. The upper limit of equalization is usually chosen to be the base of the mixed layer, since the density above this point is quite uniform, as is the density of the pressure case. Pressurization of the actual gas volume, $\gamma\beta V_{p0} = V_{g\max}$, to the pressure at the base of the mixed layer makes this depth the upper limit of equalization.

A profiling range of 0–400 m suggests a standard depth of 200 m, with a standard temperature $T_0 = 282$ K given by a typical California current temperature profile. A typical mixed layer base temperature is 289 K, typical pressure is 0.5 MPa. Calculation yields $\beta = 8.7 \times 10^{-4}$, $\gamma = 2.56$, and V_{p0} of 80 L gives a gas volume of 180 ml (Duda, 1986).

The gas volume is in the form of a cylinder of 39.3 mm bore sealed with a piston. One side of the piston is exposed to ambient pressure. The piston is captured when the gas has expanded to 180 ml. The O-ring seal of the two piece, hollow piston is lubricated with oil forced out from within the piston. The gas volume is pressurized with a regulated gas bottle before the instrument is launched.

As of May 1987 the longest deployment of a Cartesian diver has been about 48 hours, with 34 dives to 350 m. One diver has completed about 120 profiles during 7 trips. No problems with the buoyancy changers has been encountered, and no overhaul has been made with the exception of replacement of an electric motor whose brushes wore out during software testing and added sufficient RF noise to crash the computer system. It is not certain whether the mechanism could last for a 200 dive deployment, but we judge it likely. The compressibility equalizer seems to jam on occasion, rendering it useless. Because it is not essential for dives to 350 m or less, and because no deep dives have been made, the seal of the passive piston has not been redesigned.

c. Profiling of horizontal velocity

The inductive current measuring system, which will be called the Geomagnetic Electrokinetograph (GEK) after von Arx (1950), has seen successful application

in the last decade. Our instrument differs from the geomagnetic inductive profilers of Sanford et al. (1978) and those of Sanford et al. (1982) by measuring the electric field away from the body of the instrument, instead of one perturbed by the presence of the instrument, and while moving horizontally with the water, rather than at a different velocity. This inductive field measurement technique corresponds to the case I instrument in the discussion of Sanford et al. (1978).

A vertically moving case I instrument can be interpreted as responding to three distinct electromotive forces (emfs). One emf is due to the electric field which corresponds, through Ohm's law, to the local electric current in the seawater. The vertical structure of that current is induced by local seawater motion through the magnetic field of the earth (Sanford, 1971). Errors in the calculation of current profiles from electric field measurements will be discussed here. The second emf is due to the horizontal velocity of the instrument relative to the surrounding fluid. The third emf is due to the vertical velocity of the instrument relative to the geomagnetic field. For a horizontally Lagrangian case I instrument, like the Cartesian diver, the second emf vanishes, leaving only the emf coupled to the oceanic velocity field and the emf induced by the vertical motion of the electrode pairs. Calculation based on the work of Sanford et al. (1978) shows that the Cartesian diver electrodes are sufficiently far from the insulated pressure case to cause only a 2% deviation from an ideal case I instrument. The calculation is outlined in the Appendix.

One can also interpret the ideal case I instrument as measuring the velocity of its electrode pairs relative to the geomagnetic field. Therefore, the diver measures something very near its own velocity. Oceanic velocities are obtained if the diver moves as a Lagrangian tracer in the horizontal. Since the ship towed GEK system of von Arx (1950) measured its own velocity, the case I instrument is a GEK, while the other cases are not.

For the case I instrument measuring the unperturbed field, the governing expression is Ohm's law for a moving medium,

$$\mathbf{J} = \sigma(\mathbf{E}_s + \mathbf{V} \times \mathbf{F}) = \sigma \mathbf{E}', \tag{9}$$

where $\mathbf{J}$ is the electric-current density, σ the conductivity of the surrounding water, $\mathbf{E}_s$ the electric field in a stationary reference frame, $\mathbf{V}$ the velocity of the electrode pair (the instrument), and $\mathbf{F}$ the geomagnetic induction. $\mathbf{E}'$ is the electric field in the reference frame moving with the electrodes. Variations with depth of $\mathbf{E}'$ are measured by the Cartesian diver.

The relationship of this field to internal-wave velocity $\mathbf{U} = \mathbf{u}(z) \exp(ikx - i\omega t)$ will now be addressed. More detail can be found in Sanford (1971) and Chave (1984). From Maxwell's equations in the quasi-static limit and Ohm's law we derive an expression for magnetic induction in a conducting, moving medium:

$$-\nabla^2 \mathbf{B} + \mu\sigma \frac{\partial \mathbf{B}}{\partial t} = \mu\sigma \nabla \times [\mathbf{U} \times (\mathbf{F} + \mathbf{B})], \tag{10}$$

where $\mathbf{B}$ is the magnetic induction generated by the water motion (Cox et al., 1970); $\mathbf{B}$ can be neglected on the right-hand side of the equation, since the total induction is essentially $\mathbf{F}$. Solution of this will yield electric current density through

$$\mathbf{J} = \frac{\nabla \times \mathbf{B}}{\mu}. \tag{11}$$

Consider a right-hand Cartesian coordinate system with $\mathbf{i}$ in the direction of horizontal propagation of a sinusoidal internal-wave induced magnetic induction, $\mathbf{B} = \mathbf{b}(z) \exp(ikx - i\omega t)$, and $\mathbf{k}$ pointing upward. Let (F_z, F_y, F_z) be the components of the geomagnetic field in this system, so that $F_z = \cos\theta F_H$; F_H is the horizontal component of F; θ is the angle between the direction of propagation and magnetic north. In an ocean within which the buoyancy frequency N varies slowly in the WKB sense both horizontally and vertically, the dominant horizontal electric field due to an internal wave of wavenumber $\mathbf{q} = \mathbf{i}k + \mathbf{k}m$ and frequency ω is

$$\mathbf{E}'(k, \omega, z) = \mathbf{i}\left[\frac{-F_x ik}{m^2 + k^2} \frac{\partial v}{\partial z} + \frac{m^2 F_z v}{m^2 + k^2}\right] + \mathbf{j}[F_x w - F_z u]. \tag{12}$$

This is derived from the particular solution to (10); u, v, $w(k, \omega, z)$ are sinusoidal wave velocities in the $\mathbf{i}$, $\mathbf{j}$ and $\mathbf{k}$ directions.

Also present are electric fields associated with solutions of the homogeneous form of (10), which are required to meet the boundary condition that $\mathbf{n} \cdot \mathbf{J} = 0$ at surfaces of discontinuity of σ. $\mathbf{n}$ is the unit normal at the surface. These fields have the forms $\exp(kz)$ and $\exp(-kz)$, and have maximum amplitudes similar to the fields given by (12). The vertical gradients of these fields are weaker than those of the fields given in (12) by a factor k/m, and can be considered independent of z. A statistical test of this reasoning was made. For an ocean containing internal waves characterized by the Garrett–Munk model spectrum (Munk, 1981), the ratio of the integral of the vertical wavenumber m spectrum of these fields to the integral of the m spectrum of the solutions expressed in (12) is roughly 10^{-2}. Therefore, the boundary condition terms can be neglected.

In the same coordinate system, a simplified form of the depth-dependent horizontal portion of (9) is used for velocity estimation from the electric field,

$$\mathbf{E}'(z) = \mathbf{i}F_z V(z) - \mathbf{j}F_z U(z). \tag{13}$$

We assume the field $\mathbf{E}_s$ to be constant with depth; U, V and W are coordinates of $\mathbf{V}(z)$. $W(z) \equiv 0$ is set, representing a steadily falling instrument. If the diver is assumed to be horizontally Lagrangian, then $U = u$

and $V = v$. Differences between (12) and the new form of (13), after the substitution, are depth dependent contributions to $\mathbf{E}_s$ which contribute to error.

The error term due to vertical velocity w is small for all but high frequency internal waves, as is the difference in the $F_z v$ term. These waves (near the stability frequency N) have been observed to be weak relative to waves of low frequency (near the inertial frequency f) in the ocean. Therefore, these error terms are small. The out of phase (first) term is not significant since v and k tend to cancel. Terms which include F_y do not appear due to conservation of mass in this two-dimensional plane-wave solution. The w and the out of phase error terms are seen to cancel altogether for a wave in the magnetic east direction. This anisotropy of internal wave induced EM fields is noted by Chave (1984). Note that if $W(z)$ is measured, then the $F_x w$ term can be calculated and added to (13), reducing the error.

The assumption of Lagrangian horizontal drift is crucial for the velocity measurement. Clearly, any deviation from Lagrangian drift will contribute to error. The large wing sections and large horizontal area of the package, as well as its slow descent rate, allow this interpretation down to 10 m vertical wavelength. Analysis of diver response to shear is discussed later in this section. Two orthogonal components of emf are recorded at 4 Hz, or once every 3 cm, avoiding aliasing. Simultaneously, the heading of the instrument is sampled. In this manner, the emf is complex modulated by the rotating instrument, to be later demodulated. At midlatitudes the signal from the vertical motion of the instrument is of the same magnitude as the signal from the horizontal motion but varies only slightly as the instrument profiles, contributing negligible error to estimates of the vertical shear of horizontal currents.

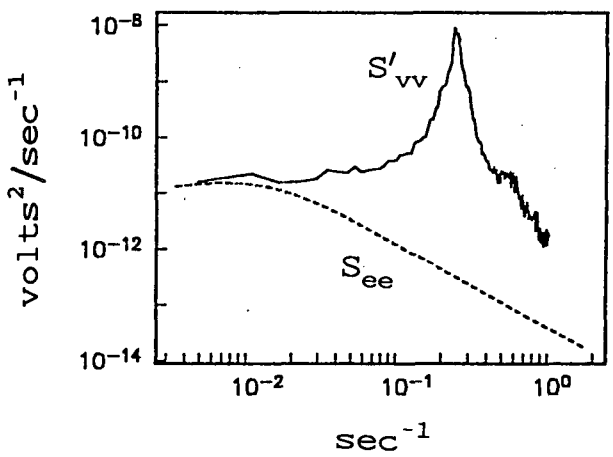

FIG. 3. Frequency autospectra of voltages input to the GEK amplifiers; S'_{vv} results in part from the vertical wavenumber spectrum of velocity in the ocean after modulation by the rotating, falling instrument, and in part from electrode noise. Data are from 14 roundtrips to 265 meters depth in the San Diego trough, 6 March 1984, up profiles only; S_{ee} is an electrode noise spectrum that fits S'_{vv} well at the noise influenced low frequencies, with $b = 2 \times 10^{-14}$.

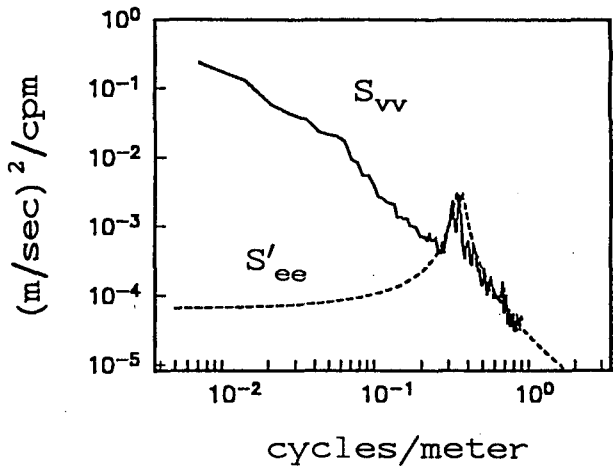

FIG. 4. The S_{vv} is a measured vertical wavenumber spectrum of horizontal velocity, calculated from S'_{vv} of Fig. 3; S'_{ee} is the apparent velocity spectrum that would result from demodulation of the electrode noise spectrum S_{ee} of Fig. 3.

The precise small-scale limit of velocity resolution, or the low-pass velocity transfer function in wavenumber space, is influenced by electrode noise and the mechanical response of the diver. Low frequency noise, of low apparent wavenumber for the profiler, is modulated into the band centered at the wavenumber corresponding to the pitch of the helix of the rotation, 3 meters. Figure 3 shows the spectra of the electrical signals that are amplified and sampled. Here S_{ee} is the high-passed electrode noise spectrum, S'_{vv} is the voltage spectrum arising from modulated (rotating) measurement of the vertical wavenumber signal spectrum, S_{vv}. The S'_{vv} spectrum shown is from 14 cycles to 265 m depth on 6 March 1984 in the San Diego trough. The noise voltage spectrum, without temperature effects, is

$$S_{ee}(\omega) = \frac{b\omega^{1/2}}{\omega_c^2 + \omega^2}, \tag{14}$$

where ω_c is the spectral corner frequency of the high-pass amplifiers and b is the spectral level of noise for an electrode pair with noise spectrum $S_{nn} = b\omega^{-1.5}$. Figure 4 shows the spectra of the same signals after demodulation; S'_{ee} is the modulated form of the electrode noise spectrum. The lowest wavenumber crossing point of the two spectra in Fig. 4 would determine the limit of resolution if the diver could respond to velocities at that scale. If, however, the limited ability of the instrument to follow vertical changes in the horizontal flow served to attenuate the velocity spectrum at wavenumbers lower than the crossover, that attenuation would determine the resolution of the velocity measurement.

Before estimating diver response to shear, tilting and wobbling of the package are considered. Sanford et al. (1982) show that tilting can introduce error voltages and thus velocity errors. For the Cartesian diver, a 1.5° tilt from the vertical would cause an error velocity equal to the least count to appear. The Cartesian diver has a static righting moment of 6 N m per degree of tilt, similar to PROTAS of Simpson (1972). Simpson estimated 0.1° as an upper bound on tilt while profiling. The vehicle of Mortensen and Lange (1976), which was winged at the tail like the rising diver, never recorded more than 0.05° of tilt with onboard accelerometers. A tilt calculation similar to that of Evans et al. (1979), with the lower end of a falling instrument accelerating with a newly encountered flow, yields an upper bound of 0.03° of tilt for the Cartesian diver in the ocean. Tilt may sometimes cause the instrument to wobble when it falls with the wings at the nose, as indicated by some noisy GEK data. Moving the wings to the center of mass may be a good idea. In addition, since the velocity of the instrument is the measured quantity, the instrument must move vertically and only vertically in a region of no flow. Asymmetries in the instrument, especially the wings, can contribute horizontal wobbling and must be suppressed to optimize the velocity measurement.

The response of falling tubes to horizontal flows has been addressed by Simpson (1972), Mortensen and Lange (1976), Carson and Simpson (1978), Evans, Rossby, Mork and Gytre (1979), and Hayes, Milburn and Ford (1984). The latter show that tilting of a fraction of a degree can influence response of the somewhat bluff TOPS profiler at profiling speeds of about 0.5 m s^{-1}. We neglect the tilt of the diver, especially for upward profiling with the wings at the tail, based initially on the measurements of Mortensen and Lange. This suitability of this assumption is confirmed by modeling, which shows that wing drag and especially lift bind the diver horizontal velocity well to that of the fluid surrounding it, and these are virtually insensitive to tilt.

Cartesian diver hydrodynamic properties in a stationary ocean are modeled using two equations, one for angular momentum about the vertical axis and one for vertical momentum. Torques included are wing lift and drag integrated radially with variable angle of attack, a length dependent drag modeled by Couette flow within a boundary layer, and drag on the salt bridges. Vertical forces are net buoyancy, radially dependent wing lift and drag, quadratic drag on the cylinder end, and inertial axial pipe drag, which is about one-half the magnitude of the end drag. For a lift coefficient one-third that of efficient airfoils (Prandtl, 1952), calculated angular and profiling velocities match within 20% those recorded in the ocean for wing inclinations of 35 to 55 deg from the horizontal. The most useful results of these calculations are estimates of the magnitudes of the wing forces.

The response to shear is determined by drag and lift which are nonlinear, so that a true wavenumber transfer function cannot be calculated. A crude response to two-dimensional velocity in layers can be obtained by amending Evans et al. (1979) equation (8) to include the forces on the wings. This is done by including lift and drag for the new angle of attack of two wings as velocity discontinuities are crossed. Two wings are assumed to have horizontal velocity normal to the shear and their diminished effect is neglected. For a chosen velocity profile, a particular realization of the transfer function results.

Four cases are simulated: rising and falling through a 4 m layer of 0.05 m s^{-1} velocity, with tube response only and tube response plus wing lift. The layer velocity and the diver velocity profiles are shown in Figs. 5a, b. The square magnitude of the spectral transfer functions for the simulations with wings are shown in Fig. 5c. Attenuation is slight at 0.1 cpm, but phase shifts (not shown) are severe for this layer model. The wing lift improves the response considerably. Since angles of attack exceed 10 degrees, this layer case is not strongly sensitive to tilt. Inspection of Figs. 4 and 5c suggests that electrode noise determines the high-wavenumber limit of velocity measurement.

The 4 Hz (3 cm) sampling rate is more frequent than required to resolve velocity features of 10 m wavelength. Furthermore, one electrode pair is sufficient for these scales of resolution, since the instrument rotates once in 3 m vertically. Having two pairs provides redundancy and a method of evaluating electrode noise levels. The cross-spectrum, coherence and phase of two sets of velocity estimates from the two pairs of electrodes are shown in Figs. 6(a, b). Figure 6(c) is the signal-to-noise ratio S for velocity calculated from one pair of electrodes, as a function of vertical wavenumber. The S can be calculated assuming uncorrelated noise of the same level for each channel, $S = R/1 - R$, where R is the coherence function between the independent velocity profiles, the normalized magnitude of the cross-spectrum. Here S is lower than the signal-to-noise ratio for velocities calculated using the voltages from both of the electrode pairs, since their noises add incoherently.

Silver–silver chloride electrodes with 5 to 25 cm^2 of exposed silver are used to measure the induced voltages. Amplification and analog to digital conversion give a least count of 0.1 microvolt, corresponding to 0.16 cm s^{-1} at 30°N latitude. The GEK amplifiers have 50k ohm input impedance, rms noise of 4.5 nanovolts between 1/30 Hz and 1/4 Hz, and consume 20 milliwatts for each of the 2 channels, including voltage to frequency conversion for digitization. For 3.1 m rotation wavelength and a typical electrode pair, the velocity noise spectrum inferred from an ocean test is shown in Fig. 4. The noise integrates to 0.6 cm s^{-1} rms in the band below 0.2 cycles per meter.

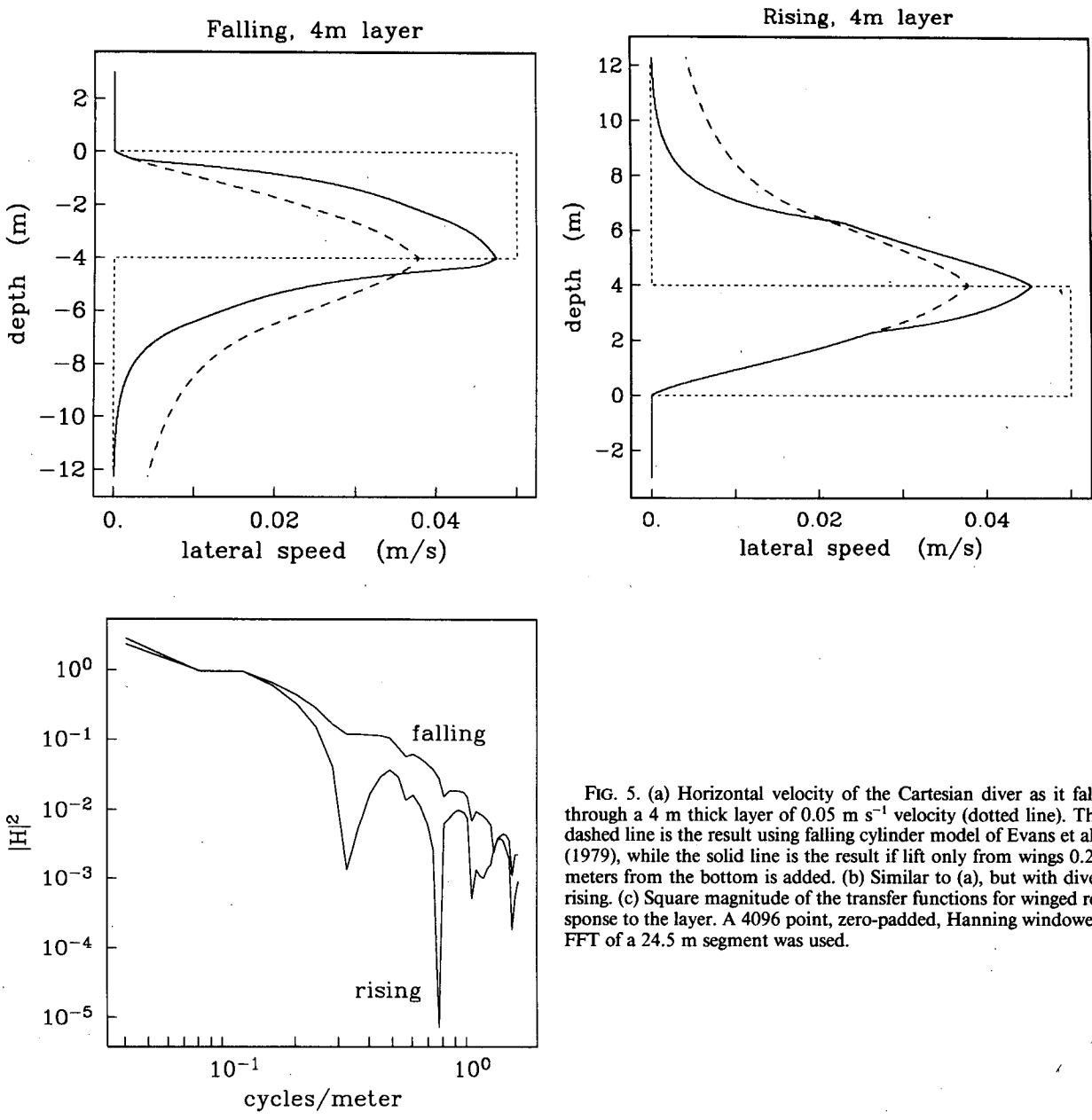

FIG. 5. (a) Horizontal velocity of the Cartesian diver as it falls through a 4 m thick layer of 0.05 m s^{-1} velocity (dotted line). The dashed line is the result using falling cylinder model of Evans et al., (1979), while the solid line is the result if lift only from wings 0.25 meters from the bottom is added. (b) Similar to (a), but with diver rising. (c) Square magnitude of the transfer functions for winged response to the layer. A 4096 point, zero-padded, Hanning windowed FFT of a 24.5 m segment was used.

Instrument orientation is determined with an 8-bit optical heading sensor. This compass is damped with silicone fluid and the indicated heading lags behind the actual heading of the rotating instrument. The internal temperature of the instrument is recorded and used to estimate the viscosity of the fluid and the lag. At the 4 Hz sampling rate, the voltages are multiplied by the sine and cosine of the diver's heading, producing four smoothly varying demodulated series. These series are autoregressively low-pass filtered and the output is sampled at 0.25 Hz, providing two velocity measurements per meter.

d. Temperature, conductivity and pressure measurement

Temperature and conductivity are measured with probes and electronics of our own design, except for a commercial nickel-iron alloy temperature sensor. The diver computer system can be reprogrammed to record any sort of data on any number of channels. The signals from all of the sensors are passed through bulkhead electrical connectors. Therefore, interchanging of probes and circuitry or installation of alternate designs can be easily accomplished.

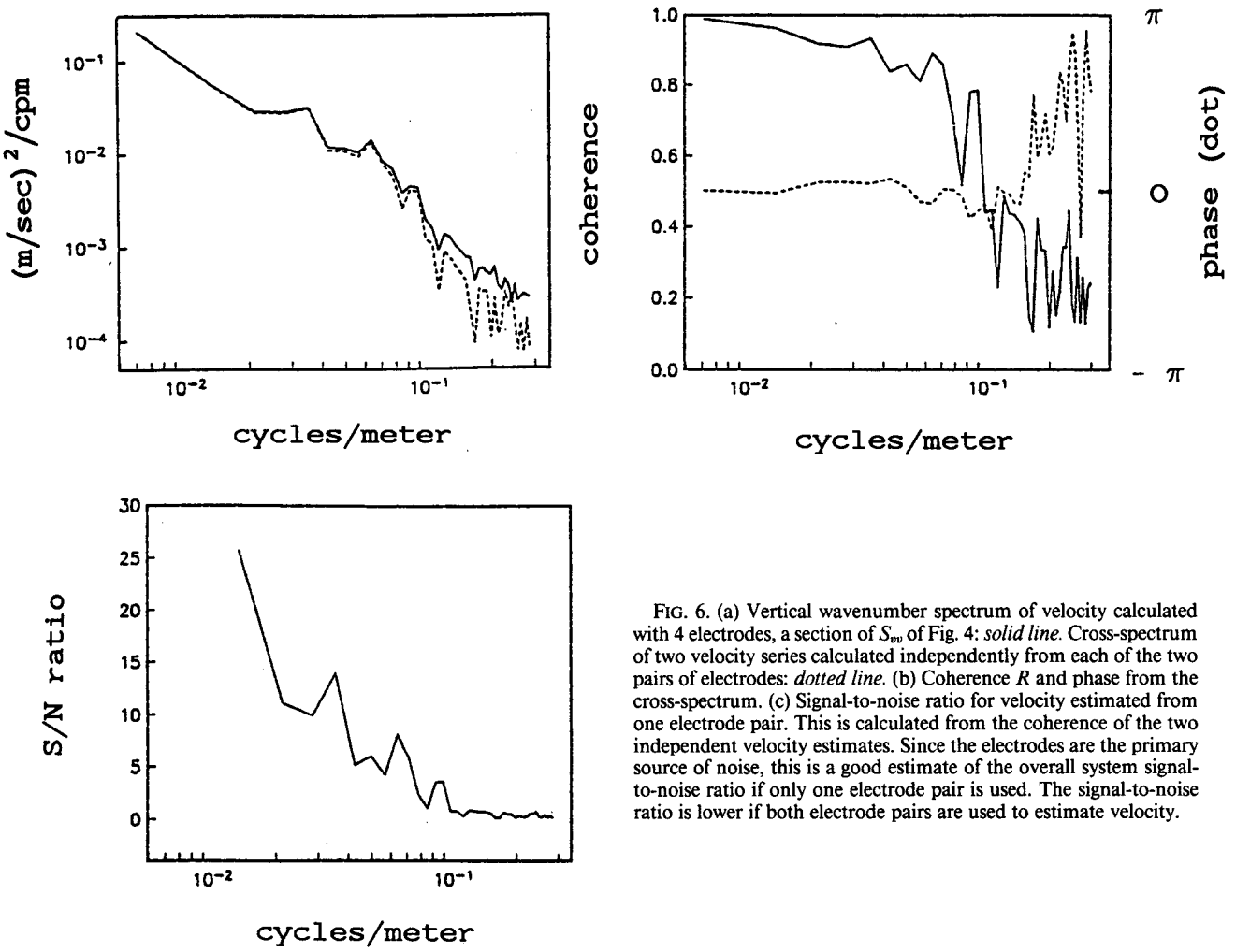

FIG. 6. (a) Vertical wavenumber spectrum of velocity calculated with 4 electrodes, a section of S_{vv} of Fig. 4: *solid line.* Cross-spectrum of two velocity series calculated independently from each of the two pairs of electrodes: *dotted line.* (b) Coherence R and phase from the cross-spectrum. (c) Signal-to-noise ratio for velocity estimated from one electrode pair. This is calculated from the coherence of the two independent velocity estimates. Since the electrodes are the primary source of noise, this is a good estimate of the overall system signal-to-noise ratio if only one electrode pair is used. The signal-to-noise ratio is lower if both electrode pairs are used to estimate velocity.

Metal resistance temperature sensors have good stability, high linearity but low sensitivity compared to thermistors. The diver alloy sensor is installed in an aluminum pressure housing, with a thermal time constant of 5 seconds, appropriate for the 0.5 m sampling used to date. The element is continually powered with 38 μA and has a resistance of 620 ohms nominally, so it dissipates 10 nanowatts for little self-heating. The least count has been set at 4.7 millidegree C and 2.6 millidegree C on different occasions. Due to the excellent linearity of the sensor, absolute accuracy over the entire range of measurement is determined by the accuracy of a two-point calibration. Root-mean-square noise level of the circuit has not been accurately determined but is known to be less than 0.5 millidegree C, or 1.5 millidegree C peak to peak in the 0.016–0.125 Hz band.

Conductivity is measured with a low power four electrode cell (Fig. 7). This type of cell has two electrodes providing an electric current which flows through a volume of water. Two sensor electrodes measure the voltage between two points on the boundary of that volume. The voltage to current ratio varies as the water conductivity changes. The diver cell has a high ratio of signal voltage to driving voltage, and has a high sample volume resistance, yielding a high signal level with low power consumption. The circuit is a feedback loop designed to keep the sensed voltage constant, with the recorded output proportional to the current supplied. Noise is introduced by the sensing electrodes and by the electronic components.

Electrodes are of platinum, while the remainder of the cell is made of 96% silica glass tubing with high dimensional stability under changing pressure and temperature. Two tubes are used, 10 cm long, 2.3 mm bore, 7.7 mm o.d., (Fig. 7). The conductivity measured is virtually that of the water within the tubes, which is flushed continuously as the diver profiles. The cell has roughly 3400 ohms resistance due to water at 4.0 S m^{-1} (40 mmho cm^{-1}), but has a slow thermal time

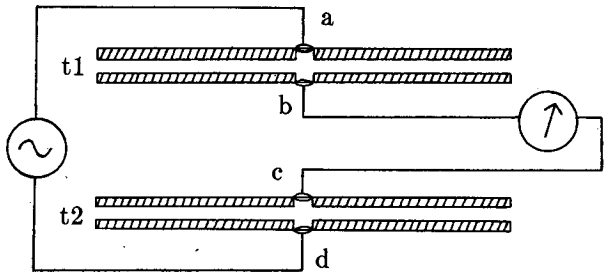

FIG. 7. Low-power conductivity probe. Two glass tubes, t1 and t2, are perforated at midpoints for electrodes a, b, c, d. Electrodes a and d are excited by the constant current ac supply. The voltage difference between sensing electrodes b and c is proportional to the resistance of the water filling the tubes.

constant of 3 seconds. Flow through the cell is unrestricted and does not influence the response, unless the cell is stalled due to misalignment with the flow. In the upper ocean with conductivity 4.0 S m^{-1}, the current required for a 1 volt cell voltage drop is about 300 μA ac. Frequency of operation is 2048 Hz. Gain has been set so that full scale is 1.06 S m^{-1}, least count 2.6×10^{-4} S m^{-1}.

Both conductivity and temperature are sampled at 4 Hz. In order to eliminate phase shift between density and velocity data, both the conductivity and temperature signals are autoregressively low-pass filtered in the same manner as the velocity series. The filter output is sampled and stored at 0.25 Hz, as with velocity.

The 3-second thermal time constant of the cell, due to the large amount of glass, is adequate to allow determination of salinity at 0.25 Hz, roughly 0.5 m. A faster cell would be required for smaller sampling intervals. Power consumption is not a problem for the diver, so a faster cell with higher power consumption can be substituted. The efficient diver cell is better suited for less frequent, long duration remote sampling. Conductivity measurement with this cell every few minutes from a mooring would be possible, since internal-wave flows of a few centimeters per second would sufficiently flush the water sample volumes in the tubes.

Pressure is determined with a strain gauge pressure transducer. Pressure range is 0–6.9 MPa (675 m ocean depth). The transducer is temperature compensated. Noise for the circuitry and bridge is equivalent to 250 Pa rms in the frequency band between 0.05 and 1 Hz. As with GEK and density, the pressure is sampled at 4 hertz. The data is low pass filtered by the computer, with the output sampled and stored at 0.25 hertz.

Vertical velocity of the surrounding water can be determined by observing both the rotation of the diver and its rate of change of depth (pressure). The least count levels of the compass and the pressure circuits for one test deployment gave a least count level of 3 mm s^{-1} for vertical velocity. Data from this experiment give self-consistent estimates of low-passed vertical velocity from slightly before and slightly after instrument turnaround, indicating that the measurement was real at wavelengths greater than 30 m. However, to use this measurement to calculate Reynolds stress, for example, different sensors are required.

Work is underway on a higher gain pressure gauge and an angular accelerometer made with a strain-gauge pressure transducer. Using these two devices, variations of the angle of attack on the wings due to ocean vertical velocity and small variations in rate of change of pressure can be monitored. Horizontal shear should not influence the rotation and fall rates of the diver due to its vertical axisymmetry, the x pattern of wings, and the near zero angle of attack expected for the wings in oceanic shear flows. Use of the diver dynamic model mentioned in section 2c may be required to interpret properly these measurements, since the diver may encounter internal wave vertical straining of sufficient magnitude to cause angular acceleration. Angular acceleration has not been large enough to detect with the 256 bit compass.

e. Microscale conductivity

To measure possible correlation between finescale velocity and density features and patterns of microscale variability, the Cartesian diver is equipped with a small conductivity cell. Washburn and Deaton (1986) described this cell and the theory of its operation. A synopsis of their discussion will be presented here, along with a description of spectral estimation circuitry included in the diver. The primary function of the microscale conductivity system is to obtain time–depth maps of evolving temperature gradient variance.

The microscale conductivity probe is a four electrode cell open in design, simply being a ceramic chip with two platinum black or rough gold plated electrodes on each side. The probe measures the resistivity of water surrounding it by driving an electric current through the water and simultaneously measuring the voltage difference between two points in the associated electric field. The electrodes function in pairs, one pair supplying electric current, the other pair measuring the voltage. Each side of the chip has one current electrode and one voltage sensor electrode.

Since the electric field in the seawater due to the current flow must penetrate the plane of the chip, the sensors sense a greater fraction of the total voltage drop than those on the probe of Washburn and Gibson (1982). This gives an improved signal to noise ratio for a particular applied power. The current supplied is a 10 mA amplitude near-sinusoid at 4.0 kHz, and about 1.25 V appears across the cell volume and the driven electrodes in 4.8 S m^{-1} water (35 ppt, 23°C). The cell resistance of the probe is defined as the sensed voltage divided by the drive current, with a higher value giving a higher signal level. Twenty-five percent of the drive

voltage is sensed, giving a cell resistance of 30 ohms in 4.8 S m^{-1} water. For comparison, a Neil Brown Instruments CTD cell has a cell resistance of 110 ohms. A low-noise constant-current source is the basis of the high-pass high-gain circuitry. It has been our experience that this allows lower noise at high frequency than constant voltage feedback designs. Noise in the band 0.5–32 Hz (320–5 mm wavelength) is equivalent to 30 μdeg C rms.

Two sampling schemes have been used for microscale conductivity. One is direct sampling of the 0.05–32 Hz band-limited signal at 64 Hz. The other is compression of the signal into temperature gradient spectral estimates for six bands. The interpretation of conductivity gradient variance as temperature gradient variance is complicated by salinity contributions to conductivity gradient variance. This may introduce an error up to a factor of 4 in temperature gradient variance estimates for realistic temperature–salinity relations, but this error is generally much less (L. Washburn, personal communication).

In the 64 Hz direct sampling scheme, the least count is 2×10^{-5} S m^{-1}. In temperature units this is 1.8×10^{-4} °C, assuming constant salinity, usually a reasonable assumption in the ocean. The 64 Hz sampling of the time series means that 700 kilobytes of conductivity data must be stored for each kilometer profiled. This is near the 1.3 megabyte internal storage capacity, so the second sampling technique is used for long deployments with repeated profiles.

In the second scheme, the signal is differentiated and input to six band-pass filters with pass bands centered at 0.75, 1.5, 3, 6, 12 and 24 Hz. Each band extends ±33% of the center frequency. For the probe speed of 0.16 m s^{-1} these bands correspond to fluctuation wavelengths from 3–200 cycles m^{-1}. The output of the filters is rectified and low pass filtered with a time constant of 6 seconds, corresponding to 0.75 m depth. The low-passed, rectified filter outputs are each sampled at 0.25 Hz, or every 0.5 meter. The rectifier output is the average absolute value of the signal. If the filter outputs are Gaussian over the 4 sec (0.5 m) sampling interval, as we assume, the six rectifier outputs can be converted to rms amplitude by multiplying by $(\pi/2)^{1/2} = 1.25$, then to power spectral estimates by squaring. These conductivity gradient spectral estimates are closely related to temperature gradient spectral estimates in the measurement band.

From these spectral estimates, an order of magnitude estimate of the local rate of turbulent kinetic energy dissipation can be made using the technique of Dillon and Caldwell (1980). The conductivity noise level of 30μ°C rms contributes a gradient noise variance of 1.2×10^{-7} (S m^{-2})^2. The smallest variance measured to date has been 3.0×10^{-7} (S m^{-2})^2, or 3.4×10^{-11} (K^2 s^{-1}) in the units of temperature dissipation rate χ. This noise level is satisfactory for studies in the upper 300 m of the ocean, but below that depth the level of variance is likely to be near the noise level much of the time. Compared to thermistors, the microscale conductivity measurement provides better resolution of small features at the expense of a slightly higher noise level. The noise in this system is determined by the constant current source. However, the lower temperature coefficient of resistance of water than that of thermistor material would reduce the signal-to-noise ratio, relative to a thermistor measurement, even for a perfectly constant current source, due to reduced voltage signal level.

f. Computer system and power supply

The computer system controls the buoyancy changer, the collection and processing of sensor signals, and the recording of data on magnetic tape. The currently installed system uses an IM6100 CMOS microprocessor and all CMOS digital circuitry. Power consumption is 100 mW with a 1 MHz clock rate.

The magnetic tape recorder is a digital cassette tape transport with stop–start capability. Capacity is 1.3 megabytes. This allows storage of 15 twelve-bit channels for 64 hours at 0.25 Hz sampling. Analog data from each amplifier is converted to frequency modulated data with voltage controlled oscillators and digitized by counting for ¼ second. These 4 Hz data are filtered by the computer system in the final 0.25 Hz data. An exception is 64 Hz digitization and direct transfer to storage of microconductivity data during short deployments.

Ninety-six D-size alkaline cells, about 12.1 kg, provide piston motor power. These are arranged to initially provide 36 volts; 30 kHz and 10 kHz switching regulators provide 27 volts dc for the motor and brake. At typical operating temperatures the cells will power at least 240 cycles to 350 meters depth, occupying 15 days at 0.12 m s^{-1} velocity. End of life has been defined to be a potential of 24 volts.

Three independent supplies, totaling thirty-three alkaline D-cells, provide 22.5 volts for the tape drive and ±9 volts for the electronics. The 9 volt supplies have the shortest operating time. Six alkaline D-cells for −9 V and twelve for +9 V will last about 3 days. Nine 3 V lithium D-cells would last roughly 24 days.

3. Observations

During the Mixed Layer Dynamics Experiment (MILDEX) of 1983 off the coast of California, the computer equipped diver collected finescale (3–200 m wavelength) velocity and temperature data, and microscale conductivity data. The data were collected on 5 November 1983, 7.2 km east of FLIP. The location was 34°09.6′N, 125°31.5′W. Figure 8 shows consecutive spectral estimates for microconductivity gradient for a falling profile. They are sampled each 0.5 m, with

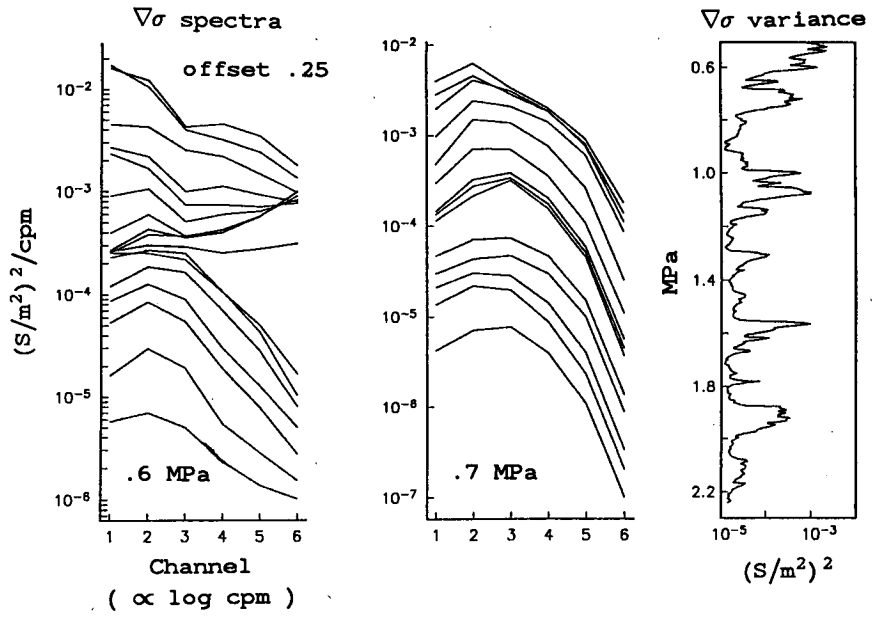

FIG. 8. Examples of twice per meter sampling of the conductivity gradient spectrum, which for this band is a good approximation of the temperature gradient spectrum. Data are for a strongly dissipative (0.6 MPa) and a moderately dissipative section of a MILDEX down profile, also shown. Each up-offset spectrum is the next deeper estimate in the ocean.

each subsequent spectrum offset $10^{0.25}$ up the diagram. The data from 0.6 MPa shows energetic straining of the temperature field to diffusive scales, presumably by near-viscous scale velocity structure according to the theory of Batchelor (1959), while the data from 0.7 MPa shows weaker but still recognizable diffusive scale activity.

The same diver was deployed over the four-day period of 10–13 August 1984. The experiment was centered 55 n.mi. offshore of Pt. Buchon, near San Luis Obispo, California at the location 35°5′N, 121°50′W. Thirty-seven round-trip profiles of velocity, temperature, and microscale conductivity activity were collected near this location in two deployments of the diver. Figure 9 shows microscale conductivity gradient variance and peak location for two consecutive round trips. The noise level is lower than that of MILDEX due to better offset elimination in the bandpass rectifier

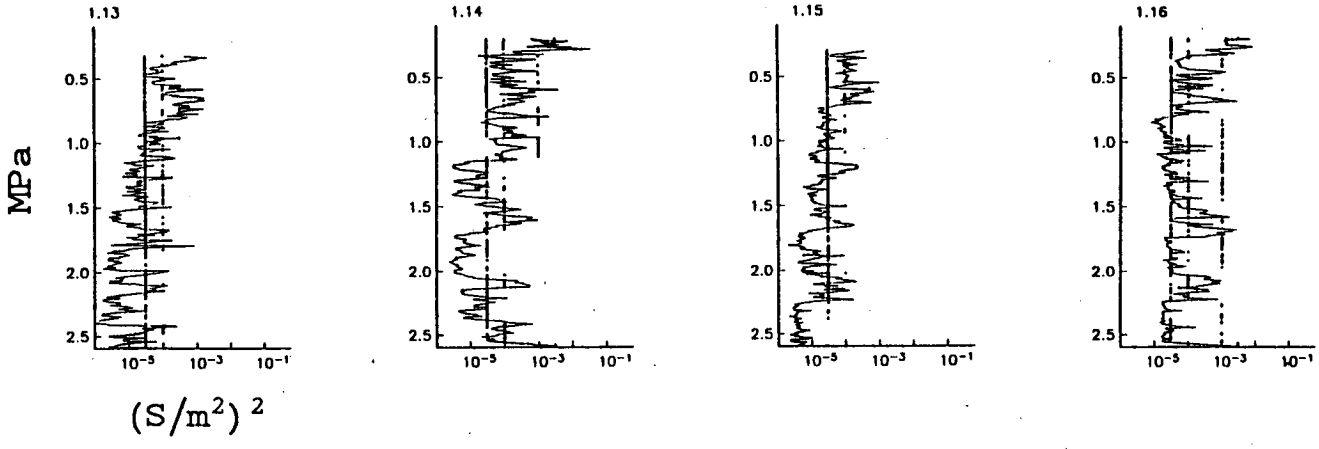

FIG. 9. Four profiles of microconductivity gradient variance, with dots indicating the wavenumber band of the highest spectral level. Variance is for the band between 3 and 200 cycles per meter. Profiles are down, up, down, up. Data are from the central California coast, near a coastal front. Dots at 3×10^{-5} indicate spectral peaks in the 6–12 cpm band, dots at 10^{-4} indicate peaks at 12–24 cpm, and so on, with dots at 3×10^{-3} indicating peaks at 100–200 cpm (unresolved spectral peak). Any peak at 3–6 cpm is disregarded, and peaks are only indicated if the spectral estimates from each channel are well above the noise level.

circuitry. Note the persistent high wavenumber and high variance activity at 1.1–1.2 MPa, and note the noisy data of the second ascent which is probably due to physical probe fouling.

Figure 10 shows 14 consecutive rising profiles collected in the San Diego trough on 6–7 March 1984. Launch was at 32°41.2'N, 117°36.0'W, with recovery 19 hours later at 32°42.1'N, 117°39.1'W. The high-wavenumber electrode noise has been digitally filtered out. The filter has a unity transfer function for wavelengths greater than 5.8 m, rolling off to −30 dB at 3.9 m. The unfiltered profiles were Fourier transformed to form the power spectrum shown in Fig. 4. The shear squared,

$$S^2 = \left(\frac{\partial U}{\partial z}\right)^2 + \left(\frac{\partial V}{\partial z}\right)^2, \qquad (15)$$

calculated from the filtered profiles is shown in Fig. 11. The S^2 scale has been expanded for depths greater than 1.1 MPa since lower shear is encountered.

The enclosed data of Figs. 10 and 11 are examined in Figs. 12 and 13. In Fig. 12, an intensifying shear feature can be seen in both components of velocity, while the successive temperature profiles show that the region of shear is being advected downward. The temperature profiles also suggest a vertically convergent flow. The projections of velocity show a clockwise rotation with depth that tightens with time, indicating that energy is propagating downward at the wavelength scale of the picture, less than 15 m. The shear is seen to increase over the 2 hour sequence, but does not resemble parallel shear flow at any scale. Instead, the shear is distributed in all directions over a scale of a few meters. Figure 13 illustrates a feature with a hodograph showing much less rotation of velocity as the feature is traversed. The linear nature of the hodograph, along with the relatively linear projection of the locally enhanced shear is not indicative of a single propagating quasi-inertial buoyancy wave.

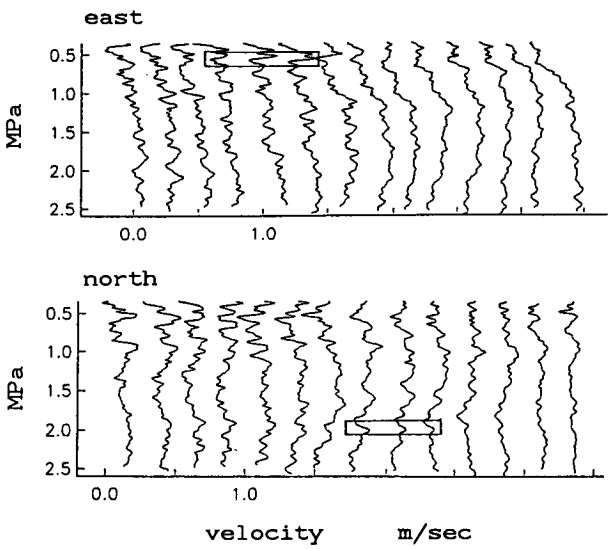

FIG. 10. Fourteen consecutive velocity profiles from the San Diego trough, collected in 15 hours. Only data taken while the instrument rising are shown. The boxes enclose regions expanded in Figs. 12 and 13.

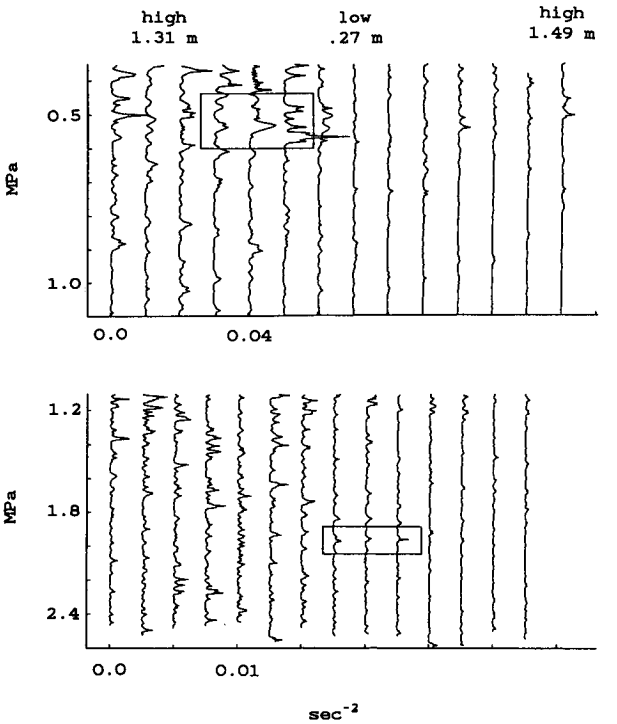

FIG. 11. Shear squared calculated from the hourly profiles of Fig. 10. Corresponding San Diego tidal extrema, in meters above mean lower low water, are indicated. The diminishing of shear over the course of the record may be associated with internal tidal flow across and along the 40 km long, 1000 m deep San Diego trough.

4. Summary

The Cartesian diver Lagrangian velocity profiler measures simultaneous profiles of density, baroclinic horizontal velocity, and 3–200 cpm conductivity gradient variance. Uninterrupted, repeated profiling is accomplished by changing the volume of the instrument between two preset values, one with positive buoyancy and one with negative. The instrument must spin as it profiles in order to measure velocity with the technique of electromagnetic induction, and the spin rate has been maximized to improve data quality. The instrument is controlled by an onboard microcomputer, which allows flexibility in profiling, type and rate of data collection, and data reduction before storage on magnetic tape. Data storage constraints prohibit collection of raw microscale data, but analog processing compresses the data before storage, saving spectral estimates at 0.5 m

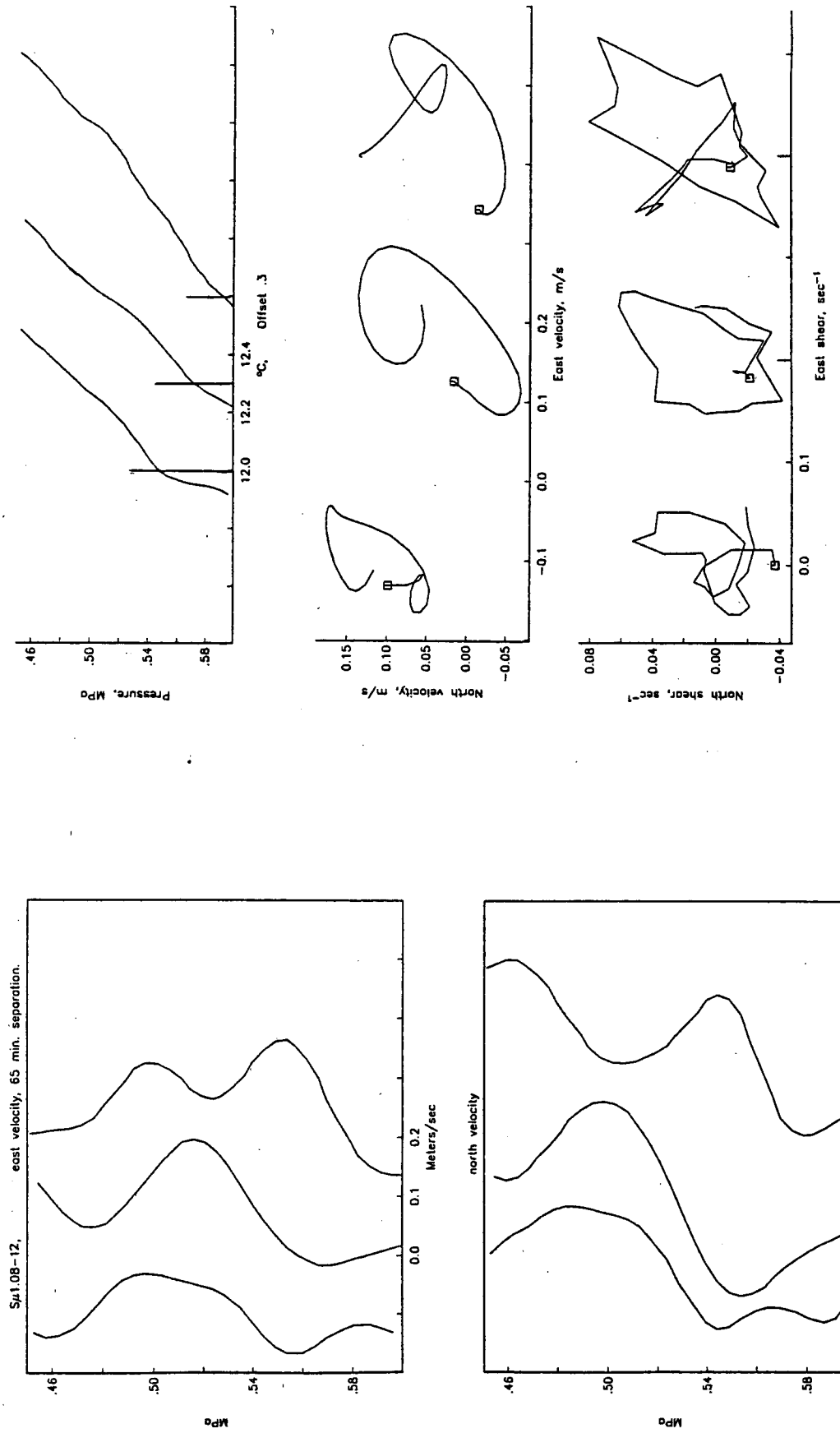

FIG. 12. A short section of three consecutive profiles, which are spaced 65 minutes apart in time. The strongest shear, extending over only a few meters vertically, intensifies with time. The temperature data show that it is being advected downward, rather than propagating downward. The boxes at the tails of the velocity and shear projections indicate the deeper end.

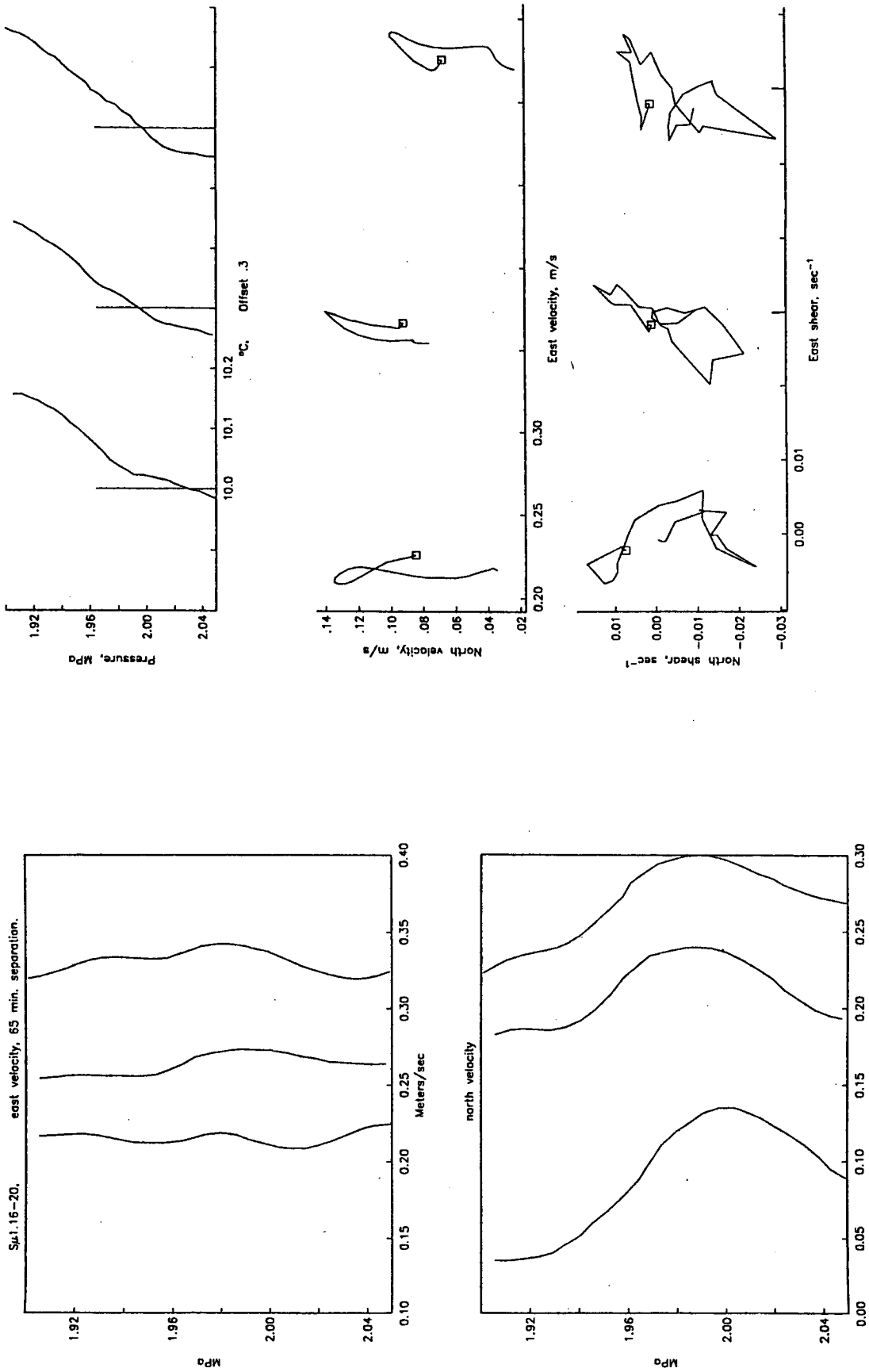

FIG. 13. Similar to Fig. 12. This shear region shows little velocity rotation with depth, and the shear intensity changes little over two hours. The 0.05 m s^{-1} northward velocity feature is very stable with time, showing the quality of the measurements.

intervals, the same interval as velocity and density sampling.

An important feature of the diver is that since the small scale limit of velocity resolution is near 10 m wavelength, most velocity features due to internal waves are recorded. This, coupled with the ability to carry microscale probes, allows the Cartesian diver to provide data potentially useful in the study of the generation of ocean turbulence from internal waves. Another important feature is the ability to determine statistical differences between internal wavefield and microstructure properties in different limited fluid volumes, made possible by Lagrangian measurement.

Acknowledgments. The Office of Naval Research has provided funding for the development and the deployment of the Cartesian diver. The UCSD Marine Sciences Development Shop performed most of the fabrication. Mike Monaco did much of the work on the electronics and the software. Clancy Latham and John Lyons helped with mechanical design and fabrication.

APPENDIX

Perturbation of an Otherwise Uniform Electric Field Near the Pressure Case

To evaluate whether the diver can be considered a true case I inductive profiler, the perturbation of a uniform electric field at the electrode locations near the insulated pressure case must be calculated. A case I instrument is one that measures its own velocity through the geomagnetic field, and does so by measuring the ocean ambient electric field uninfluenced by the presence of the instrument. The electrodes must be beyond the range of the perturbation field caused by boundary conditions at the case.

Sanford et al., (1978) derive an expression for the perturbation of an electric potential field, uniform at infinity, near an elongated spheroidal insulating body. Prolate spheroidal coordinates are used since a spheroidal body lies along a surface where one of the coordinates is constant, simplifying the problem. To apply this solution to the Cartesian diver, the assumption must be made that the shape of the diver is close enough to prolate spheroidal to make errors negligible. Since the electrode positions will be shown to be out of the perturbation field range, this approximation is justified.

The transformations from magnetic Cartesian coordinates to prolate spheroidal coordinates with focal points at $x = 0$, $y = 0$, $z = \pm a/2$ are

$$\xi = (r_1 + r_2)/a, \quad \eta = (r_1 - r_2)/a, \quad \phi = \tan^{-1} y/x; \quad \text{(A1)}$$

where

$$r_1^2 = x^2 + y^2 + (z + a/2)^2,$$

$$r_2^2 = x^2 + y^2 + (z - a/2)^2.$$

To match the coordinates to the Cartesian diver, a is set to 1.1 m. The surface of the diver will be approximated by the spheroid at $\xi = 1.02$, as was the EVMP of Sanford et al. (1978). The diver has a higher aspect ratio than the EVMP, and this is a conservatively large shape to assign to the diver. The four electrodes are at a horizontal distance 0.8 m from the z-axis, near $z = -a/2$. The approximate prolate spheroidal coordinates are

$$\xi = \sqrt{2}, \quad \eta = \sqrt{2}/2, \quad \phi = n\pi/2, \quad n \text{ integer}.$$

The distance between electrodes in each of two orthogonal pairs used to measure the horizontal components of $\mathbf{E}' = -\nabla\Phi$, 1.6 m, is denoted L. For the ideal case I instrument, $\xi \gg \xi_0$.

Within an induced field uniform at distance infinity, the solution for the potential measured by electrodes attached to a moving insulating spheroidal instrument is

$$\Phi(\xi, \eta, \phi; \xi_0) = \frac{-LF_z}{2}\{\cos\phi[(v - \bar{v})(1 + C_1) + V(1 + C_3)] - \sin\phi[(u - \bar{u})(1 + C_1) + U(1 + C_3)]\} + \frac{LF_H}{2} W(1 + C_2)\cos\phi - zF_H U(1 - C_4) \quad \text{(A2)}$$

where $\bar{u}$ and $\bar{v}$ are the conductivity weighted average east and north velocities of the water column; u and v and $w \equiv 0$ are the local water velocity Cartesian components. The U, V and W are velocity components of the instrument relative to the water, and F_H and F_z are the horizontal and vertical components of the geomagnetic induction. The coefficients C_j are functions of ξ and ξ_0.

Changes of Φ recorded while the diver profiles are of interest, since they are sensitive to changes of u and v with depth. Here U is small for the diver and W changes little with z, so the last two terms can be neglected. Terms containing $\bar{u}$ and $\bar{v}$ can also be neglected.

The C_1 and C_3 are expressed in terms of Legendre functions of the first and second kind, P_1^1, Q_1^1; and their derivatives with respect to ξ, $P_1'^1$, $Q_1'^1$:

$$C_1(\xi) = \frac{-P_1'^1(\xi_0) Q_1^1(\xi)}{Q_1'^1(\xi_0) P_1^1(\xi)}$$

$$C_3(\xi) = -\left(\frac{P_1'^1(\xi_0)}{Q_1'^1(\xi_0)}\right)^2 \frac{Q_1^1(\xi_0) Q_1^1(\xi)}{P_1^1(\xi_0) P_1^1(\xi)}. \quad \text{(A3)}$$

For $\xi = \sqrt{2}$ and $\xi_0 = 1.02$, they have values $C_1 = 0.015$ and $C_3 = -0.019$. Therefore, for the Cartesian diver

$$\Phi = \frac{-LF_z}{2}\{\cos\phi[1.015v + 0.98V] - \sin\phi[1.015u + 0.98U]\}.$$

If the electrodes were in a region uninfluenced by the presence of the pressure case, i.e., at large ξ, the

coefficients inside the brackets would be 1. In Cartesian diver data reduction, the terms in brackets are taken to be $v + V$ and $u + U$, leading to a two percent error. This error, although systematic, is considered to be negligible in comparison with electrode noise and other uncertainties.

REFERENCES

Batchelor, G. K., 1959: Small-scale variation of convected quantities like temperature in turbulent fluid: Part 1. General discussion and the case of small conductivity. *J. Fluid Mech.*, **5**, 113–133.

Cairns, J. L., and G. O. Williams, 1976: Internal wave observations from a midwater float, 2. *J. Geophys. Res.*, **81**, 1943–1950.

Carson, R. M., and J. H. Simpson, 1978: Comment on "Design considerations of wing stabilized free-fall vehicles" by A. C. Mortensen and R. E. Lange. *Deep-Sea Res.*, **25**, 577–579.

Chave, A. D., 1984: On the electromagnetic fields induced by oceanic internal waves. *J. Geophys. Res.*, **89**, 10519–10528.

Cox, C. S., J. H. Filloux and J. C. Larsen, 1970: Electromagnetic studies of ocean currents and electrical conductivity below the ocean-floor. *The Sea*, Vol. 4, Part 1, A. E. Maxwell, Ed., Wiley-Interscience, 637–693.

Dillon, T. M., and D. R. Caldwell, 1980: The Batchelor spectrum and dissipation in the upper ocean. *J. Geophys. Res.*, **85**, 1910–1916.

Duda, T. F., 1986: Observations of horizontal flow, vertical shear and microstructure in the upper ocean. Ph.D. dissertation, University of California, San Diego, 151 pp.

——, and C. S. Cox, 1987: Vorticity measurement in a region of coastal ocean eddies by observation of near-inertial oscillations. *Geophys. Res. Lett.*, **14**, 793–796.

Eriksen, C. C., J. M. Dahlen and J. T. Shillingford, Jr., 1982: An upper ocean moored current and density profiler applied to winter conditions near Bermuda. *J. Geophys. Res.*, **87**, 7879–7902.

Evans, D. L., H. T. Rossby, M. Mork and T. Gytre, 1979: YVETTE—a free fall shear profiler. *Deep-Sea Res.*, **26**, 703–718.

Filloux, J. H., 1973: Techniques and instrumentation for study of natural electromagnetic induction at sea. *Phys. Earth Planet. Int.*, **7**, 323–338.

Hayes, S. P., H. B. Milburn and E. F. Ford, 1984: TOPS: A free-fall velocity and CTD profiler. *J. Atmos. Oceanic Technol.*, **1**, 220–236.

Luyten, J. R., G. Needell and J. Thomson, 1982: An acoustic dropsonde—design, performance and evaluation. *Deep-Sea Res.*, **29**, 499–524.

Magiotti, R., 1648: *Renitenza certissima dell' acqua alla compresione dichiarata con varijscherzi in occassion d'altri problemi curioisi.*, Per Francesca Maneta, Roma [Available at the SIO library and the British Museum.]

Mortensen, A. C., and R. E. Lange, 1976: Design considerations of wing stabilized free-fall vehicles. *Deep-Sea Res.*, **23**, 1231–1240.

Munk, W. H., 1981: Internal waves and small-scale processes. *Evolution of Physical Oceanography*, B. A. Warren and C. Wunsch, Eds., The MIT Press, 264–291.

Petiau, G., and A. Dupis, 1980: Noise, temperature coefficient, and long time stability of electrodes for telluric observations. *Geophys. Prospect.*, **28**, 792–804.

Pinkel, R., 1980: Acoustic Doppler techniques. *Air-Sea Interaction, Instruments and Methods*, F. Dobson, L. Hasse and R. Davis, Eds., Plenum Press, 171–200.

Prandtl, L., 1952: *The Essentials of Fluid Dynamics*, Blackie.

Regier, L., 1982: Mesoscale current fields observed with a shipboard profiling acoustic current meter. *J. Phys. Oceanogr.*, **12**, 880–886.

Sanford, T. B., 1971: Motionally induced electric and magnetic fields in the sea. *J. Geophys. Res.*, **76**, 3476–3492.

——, R. G. Drever and J. H. Dunlap, 1978: A velocity profiler based on the principles of geomagnetic induction. *Deep-Sea Res.*, **25**, 183–200.

——, ——, —— and E. A. D'Asaro, 1982: Design, operation and performance of an expendable temperature and velocity profiler (XTVP). APL-UW 8110.

Simpson, J. H., 1972: A free fall probe for the measurement of velocity microstructure. *Deep-Sea Res.*, **19**, 331–336.

Spain, P. F., D. L. Dorson and H. T. Rossby, 1981: PEGASUS: A simple, acoustically tracked, velocity profiler. *Deep-Sea Res.*, **28**, 1553–1567.

von Arx, W. S., 1950: An electromagnetic method for measuring the velocities of ocean currents from a ship underway. *Pap. Phys. Oceanogr. Meteor.*, **II**, 1–62.

Washburn, L., and T. K. Deaton, 1986: A simple system for mapping conductivity microstructure. *J. Atmos. Oceanic Technol.*, **3**, 345–355.

——, and C. H. Gibson, 1982: Measurement of oceanic temperature microstructure using a small conductivity probe. *J. Geophys. Res.*, **87**, 4023–4040.